 FDMP, vol.10, no.1, pp.1-36, 2014

The JEREMI-Project on Thermocapillary Convection in Liquid Bridges. Part A: Overview of Particle Accumulation Structures

H. C. Kuhlmann[1], M. Lappa[2], D. Melnikov[3], R. Mukin[1], F. H. Muldoon[1], D. Pushkin[4], V. Shevtsova[2] and I. Ueno[5]

Abstract: The rapid accumulation of particles suspended in a thermocapillary liquid bridge is planned to be investigated during the JEREMI experiment on the International Space Station scheduled for 2016. An overview is given of the current status of experimental and numerical investigations of this phenomenon.

Keywords: thermocapillary flow, liquid bridge, particle accumulation, PAS.

1 Introduction

Thermocapillary flows in liquid bridges have been the subject of intense research since scientific space missions on fluid dynamics under weightlessness conditions became regularly available in the 1980's. Early ground experiments of Schwabe, Scharmann, Preisser, and Oeder (1978) have confirmed the existence of oscillatory flows in thermocapillary liquid bridges if the temperature variation along the free surface is sufficiently large. Thereafter, Schwabe and Scharmann (1979) specified the critical Marangoni number for the onset of oscillations and sketched the spatial structure of the azimuthally traveling wave. Similar results were found independently by Chun and Wuest (1979). In a sounding-rocket experiment Schwabe, Preisser, and Scharmann (1982) observed a similar scenario as on the ground. These investigations have shown that thermocapillarity is a strong natural-convection mechanism in microgravity. On the ground in millimetric liquid bridges it can dominate even buoyant convection. Over time, the system of a thermocapillary liquid bridge has become a standard problem for the study of

[1] Vienna University of Technology, Vienna, Austria
[2] Telespazio, Naples, Italy
[3] Free University of Brussels, Brussels, Belgium
[4] University of Oxford, United Kingdom
[5] Tokyo University of Science, Chiba, Japan

thermocapillary flows (Kuhlmann, 1999; Lappa, 2010; Shevtsova, Mialdun, Kawamura, Ueno, Nishino, and Lappa, 2011).

Many of the early investigations have suffered from poor control of the conditions in the ambient gas phase. This led to relatively large uncertainties in the determination of the critical Marangoni number for the onset of three-dimensional flow. The JEREMI consortium (Japanese–European Research Experiment on Marangoni Instability) is preparing a space experiment on the ISS with a launch date of 2016 in which the ambient atmosphere is much better defined. This can be accomplished by exposing the liquid bridge to a co-axial gas flow in an annular gap around the liquid bridge. This setup also allows control of the flow in the liquid zone. Of particular interest is the delay or advancement of the onset of flow oscillations which, for large-Prandtl-number liquids, typically arise as hydrothermal waves (Smith and Davis, 1983; Wanschura, Shevtsova, Kuhlmann, and Rath, 1995). The JEREMI experiment is being developed by an International Topical Team on *Marangoni instabilities in systems with cylindrical symmetry* with the support of JAXA and ESA.

In addition to controlling the flow in thermocapillary liquid bridges, the JEREMI experiment provides the opportunity to study particle accumulation structures. This phenomenon has been discovered by Schwabe, Hintz, and Frank (1996) who coined the abbreviation PAS for the rapid accumulation of particles suspended in a thermocapillary liquid bridge. Examples of PAS are shown in Fig. 1. Research on PAS is also supported by JAXA and by ESA in the context of the JEREMI project. A precursor flight on MAXUS-6 in 2004 has shown that buoyancy forces due to gravity can be excluded as the primary mechanism for PAS formation. Nevertheless, the parameters for which PAS exists do depend on the gravity level (Schwabe, Tanaka, Mizev, and Kawamura, 2006). The typical length scale of liquid bridges on the ground is limited to a few millimeters in order to prevent capillary rupture due to gravity forces. This size restriction complicates accurate measurements of the flow. The length scale is much less restricted under conditions of weightlessness, with experiments with liquid bridges of length up to 60 millimeters having been carried out successfully on the International Space Station (Kawamura, Nishino, Matsumoto, and Ueno, 2010; Yano, Nishino, Kawamura, Ueno, Matsumoto, Ohnishi, and Sakurai, 2011; Sato, Ueno, Kawamura, Nishino, Matsumoto, Ohnishi, and Sakurai, 2013). Thanks to the weightlessness environment, the JEREMI experiment enables study of PAS under conditions that are well-controlled and ideal for accurate measurements, and thereby permits relating this phenomenon to the particle and flow properties under which it exists with the aim of elucidating the mechanism(s) causing PAS.

This part A of a series of two review articles is concerned with the progress made

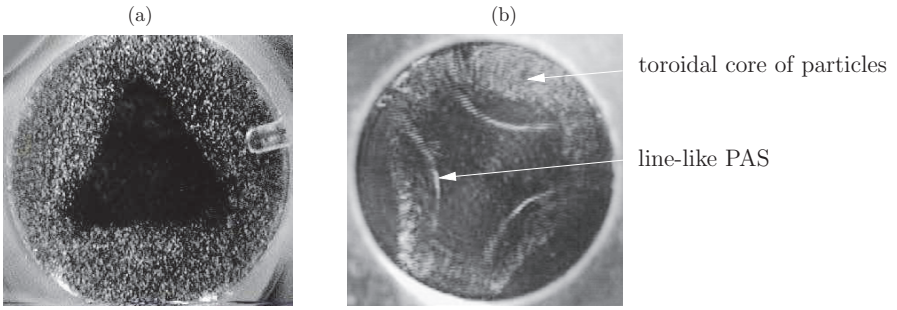

Figure 1: Examples for particle accumulation patterns viewed co-axially through a transparent heating rod. (a) Polygonal depletion zone (Kawamura, Ueno, Tanaka, and Nagano, 2001), (b) line-like PAS and toroidal core of particles. Note that the toroidal core is clipped on the left and near the bottom right due to the illumination system.

in the exploration of PAS and the related preparations of the JEREMI experiment. Part B covers the subject of thermocapillary flow control by a co-axial gas flow.

Schwabe, Hintz, and Frank (1996) have shown that particles suspended in a thermocapillary liquid bridge can segregate very rapidly and form peculiar patterns. Among the patterns observed, the most remarkable one is the organization of the majority of particles into a thin closed thread (line-like PAS visible in Fig. 1b) which winds about the core of the toroidal vortex which stems from the axisymmetric basic flow and underlies the hydrothermal wave. The accumulation structure rotates about the axis of the liquid bridge without changing its shape. The angular velocity of PAS[1] is the same as that of the hydrothermal wave. Therefore, the phase difference between PAS and the hydrothermal wave is constant, but may depend on the governing flow and particle parameters. While the particle-accumulation structure rotates about the axis, individual particles do not move along the particle thread in the laboratory frame of reference. In the temporal mean the azimuthal coordinate of an individual particle on PAS remains nearly constant. Individual particles on PAS do drift azimuthally, however, with a drift velocity much smaller than the phase velocity of PAS. This drift is caused by the azimuthal mean flow of the hydrothermal wave (Leypoldt, Kuhlmann, and Rath, 2000; Tanaka, Kawamura, Ueno, and Schwabe, 2006).

[1] If not mentioned otherwise *PAS* is used here for *line-like PAS* which would be more precise, because other variants of particle accumulation structures are the polygonal depletion zone, tubular PAS and strange PAS (Muldoon and Kuhlmann, 2013a).

After the seminal publication of Schwabe, Hintz, and Frank (1996) several experimental investigations have been carried out to explore the parameters on which PAS depends. Tanaka, Kawamura, Ueno, and Schwabe (2006) have investigated the fundamental features of PAS. They found that PAS is only observed in a traveling hydrothermal wave, not in a standing wave. It was confirmed, moreover, that PAS has the same azimuthal period as the underlying hydrothermal wave. For $\mathrm{Pr} = 28$ (2 cSt silicone oil) Tanaka, Kawamura, Ueno, and Schwabe (2006) found two different types of PAS: Spiral Loop 1 (SL-1-PAS) and Spiral Loop 2 (SL2-PAS). They also established that PAS rotates without changing its shape. In a wide range of parameters, the properties of PAS do not depend on the particle size or density. By dye injection it was shown that the shape of PAS is primarily determined by the flow field, as the dye streaks took the same shape as PAS. Noteworthy, Tanaka, Kawamura, Ueno, and Schwabe (2006) also found that the distance between the surface of the particles on PAS and the free surface is never larger than one particle radius. Two phenomena also discussed by Tanaka, Kawamura, Ueno, and Schwabe (2006) are closely related to line-like PAS: the polygonal depletion zone (Fig. 1a) and the toroidal core of particles (Fig. 1b). The latter is transient, but observable for a long time if the particle density differs not too much from that of the liquid.

Schwabe, Mizev, Udhayasankar, and Tanaka (2007) visualized the shapes of PAS using molten $NaNO_3$, $CsNO_3$ and mixtures of both. They systematically investigated the range of particle sizes, particle-to-fluid density ratios, Marangoni numbers and aspect ratios of the liquid bridge under which PAS can be observed. They found that PAS was only formed for certain ranges of the aspect ratio (height-to-radius ratio of the liquid bridge) for which a perfect traveling hydrothermal wave is realized. Optimum Marangoni numbers were found to be typically twice the critical value for the onset of the wave. The time required to form PAS after an initially unordered flow state and particle distribution took a minimum value when the density of the particles is matched to the mean density of the liquid. Moreover, the particles must be larger than a certain minimum size in order to form PAS. Depending on the relative particle density there exists an optimum particle size for which the PAS formation time has a local minimum. Typical particle diameters for which PAS can be observed in liquid bridges with radius and length of the order of 2–3 mm range from 10 to 60 microns. Thus the ratio of the length scales between particles and the flow system is of the order of 10^{-2}.

This paper is intended to provide an overview of the current knowledge and understanding of the intriguing phenomenon of PAS. After a mathematical formulation in section 2, results from the research groups participating in the JEREMI collaboration are presented in section 3. Owing to the limited space available and the various approaches used, this review cannot be comprehensive and only the main

findings can be highlighted. For that reason the reader is referred to the more detailed original research papers quoted in the text. Finally, a brief summary is given together with a view on future perspectives concerning PAS.

2 Mathematical formulation

For the subject of particle accumulation, in this part A of the paper, we shall restrict the mathematical formulation to a liquid bridge only, using a relatively simple model of the ambient conditions. A more detailed description of the ambient conditions is provided in part B, where all boundary conditions and the geometry of the gas atmosphere in an annulus surrounding the liquid bridge will be formulated and specified. This restriction seems to be justified, because PAS can also be observed without an ambient gas flow. It is obvious that the effect of the ambient conditions will modify PAS, but this modification acts indirectly through a change of the flow field in the liquid bridge.

The typical geometry of a liquid bridge consists of two coaxial cylindrical solid rods of radius R which are separated by a distance d. An important geometrical parameter is the aspect ratio $\Gamma = d/R$. If a droplet with a suitable volume is placed in the gap between the rods a liquid bridge is formed which is stabilized by surface tension. When the upper and lower rods, which should have high thermal conductivity, are heated at T_h and cooled at T_c, respectively, with a temperature difference $\Delta T = T_h - T_c$, the temperature variation along the liquid–gas interface can cause significant fluid motion via the thermocapillary effect. At small temperature differences the flow is axisymmetric. With an increase of the temperature difference the axisymmetry is broken (Wanschura, Shevtsova, Kuhlmann, and Rath, 1995) and the flow becomes three-dimensional. For a Prandtl number larger than about one this symmetry-breaking bifurcation leads to an oscillatory flow. Slightly above the threshold the flow arises either as an azimuthally traveling or as an azimuthally standing wave (Leypoldt, Kuhlmann, and Rath, 2000). Here we only consider traveling waves, because PAS has only been observed in traveling waves.

2.1 Bulk equations

The liquids used in experiments on thermocapillary convection, e.g. molten salts or silicone oils, can be modeled as Newtonian fluids. However, the temperature dependencies of the surface tension σ, of the density ρ and of the kinematic viscosity

ν are important. To first order these quantities can be expanded in Taylor series

$$\sigma = \sigma_0 - \gamma(T - T_0) + O(T - T_0)^2, \tag{1}$$

$$\rho = \rho_0 [1 - \beta (T - T_0)] + O(T - T_0)^2, \tag{2}$$

$$\nu = \nu_0 - \zeta (T - T_0) + O(T - T_0)^2, \tag{3}$$

where $T_0 = (T_h + T_c)/2$ is the arithmetic mean temperature of the cylinders, γ is the surface-tension coefficient, β the thermal expansion coefficient and ζ the Taylor coefficient of the kinematic viscosity. The reference quantities σ_0, ρ_0 and ν_0 are evaluated at the mean temperature T_0.

The variation of the surface tension is essential, as it is the primary driving force of the flow in liquid bridges. The surface-tension coefficient γ enters in the boundary conditions. In a terrestrial environment, thermal expansion is treated in the framework of the Boussinesq approximation such that density variations are only taken into account in the buoyancy body-force term. Owing to the relatively high temperature difference imposed on the cylindrical rods the kinematic viscosity may vary up to 50% with respect to its mean value. Therefore, this dependence should be taken into account in the viscous stress term.

If we use the scales d for lengths, d^2/ν_0 for time, ν_0/d for velocities, $\rho_0 d^2/\nu_0^2$ for the pressure and the dimensionless temperature $\theta = (T - T_0)/\Delta T$ we obtain the Navier–Stokes, continuity and energy equations in dimensionless form

$$\frac{\partial \vec{u}}{\partial t} + \vec{u} \cdot \nabla \vec{u} = -\nabla p + \nabla \cdot \Sigma + \mathrm{Gr}\theta \vec{e}_z, \tag{4a}$$

$$\nabla \cdot \vec{u} = 0, \tag{4b}$$

$$\frac{\partial \theta}{\partial t} + \vec{u} \cdot \nabla \theta = \frac{1}{\mathrm{Pr}} \nabla^2 \theta, \tag{4c}$$

where $\vec{u}$ and p denote the velocity and pressure fields and $\mathrm{Pr} = \nu_0/\kappa$ and $\mathrm{Gr} = \beta g \Delta T d^3/\nu_0^2$ are the Prandtl and the Grashof number, respectively, where κ is the thermal diffusivity of the liquid and g the acceleration of gravity. The quantity $\Sigma = f(\theta)\left[\nabla\vec{u} + (\nabla\vec{u})^{\mathrm{T}}\right]$ is the viscous part of the stress tensor. Here $f(\theta) = \nu(\theta)/\nu_0$ or, in linear approximation, $f(\theta) \approx 1 - \mathrm{R}_\nu \theta$ with $\mathrm{R}_\nu = \zeta \Delta T/\nu_0$ being the viscosity group.

2.2 Boundary conditions

Apart from the mean surface tension σ_0 the shape of the liquid bridge depends on the liquid volume V and on the hydrostatic pressure distribution. Typically, the dynamic flow-induced deformations are very small (Kuhlmann and Nienhüser, 2002)

and can be neglected. A good approximation of the surface shape is, therefore, given by the hydrostatic shape of the liquid bridge. The edges of the interface are assumed to be pinned to the sharp circular edges of the supporting rods.

On the plane rigid walls we assume no-slip and no-penetration boundary conditions as well as imposed temperatures with heating from above. Using cylindrical polar coordinates (r,φ,z) this leads to

$$\vec{u}(z=1/2)=\vec{u}(z=-1/2)=0, \tag{5}$$

$$\theta(z=\pm 1/2)=\pm\frac{1}{2}. \tag{6}$$

The first-order term $\sim\gamma$ in the surface tension is important, because the temperature variation of the surface tension provides the key driving mechanism of the flow via the thermocapillary effect. With the above scaling and the surface normal vector $\vec{n}$ directed out of the liquid, the thermocapillary boundary condition for the normal and tangential stresses on the free surface and the condition for the normal velocity can be written as (Kuhlmann and Nienhüser, 2003)

$$\Sigma\cdot\vec{n}=[\Sigma_a+(p-p_a)\mathsf{I}]\cdot\vec{n}-\frac{1}{\mathrm{Ca}}(\nabla\cdot\vec{n})\vec{n}+\mathrm{Re}(\mathsf{I}-\vec{n}\vec{n})\cdot\nabla\theta, \tag{7}$$

$$\vec{n}\cdot\vec{u}=0, \tag{8}$$

where I is the identity operator. The surface tension coefficient enters the Reynolds number $\mathrm{Re}=\gamma\Delta T d/(\rho_0\nu_0^2)$ and the strength of the surface tension determines the Capillary number $\mathrm{Ca}=\rho_0\nu_0^2/(\sigma_0 d)$. In many situations the viscous stresses exerted by the gas phase $\Sigma_a\cdot\vec{n}$ and the pressure variation in the ambient gas $p_a(z)$ can be neglected. However, for a strong axial flow in the surrounding annulus the pressure drop in the gas phase may dominate the hydrostatic pressure in the liquid and significantly deform the liquid bridge up to the point where it breaks (see part B).

For the temperature field which enters (7) we assume, in this part A, that Newton's law of heat transfer can be applied

$$\vec{n}\cdot\nabla\theta=-\mathrm{Bi}(\theta-\theta_a), \tag{9}$$

with the Biot number $\mathrm{Bi}=hd/k$ and an ambient temperature distribution $\theta_a(z)$, where h is the heat transfer coefficient and k the thermal conductivity of the liquid. The ambient flow can dramatically change the heat transfer and thus the free-surface temperature, such that the flow field is significantly influenced via the thermocapillary stress boundary condition (7) as this is the sole driving force acting on the liquid.

In numerical approaches the boundary conditions are frequently simplified. For instance, the shape of the liquid bridge is often taken to be cylindrical. The cylindrical shape can be obtained under zero gravity and realized approximately under terrestrial conditions, if the liquid bridge is sufficiently small. In that case the surface normal vector $\vec{n} = \vec{e}_r$ is the radial unit vector. Moreover, adiabatic conditions, $\vec{n} \cdot \nabla\theta = 0$, are frequently employed when the Biot number is small or when it is not easy to determine. In part B the phenomenological model (9) is avoided by explicitly balancing the heat fluxes on both sides of the interface.

For an overview the most important dimensionless numbers are

$$\Gamma = \frac{d}{R}, \quad \mathrm{Re} = \frac{\gamma \Delta T d}{\rho_0 \nu_0^2}, \quad \mathrm{Gr} = \frac{\beta g \Delta T d^3}{\nu_0^2}, \quad \mathrm{R}_\nu = \frac{\zeta \Delta T}{\nu_0}, \quad \mathrm{Bi} = \frac{hd}{k}, \quad \mathrm{Ca} = \frac{\rho_0 \nu_0^2}{\sigma_0 d}. \tag{10}$$

2.3 Particle transport

For PAS we consider spherical particles with a radius a and density ρ_p. The density ratio between particles and liquid is denoted $\rho = \rho_p/\rho_0$. An important quantity governing the transport of particles in a viscous liquid is the Stokes number which can be defined as

$$\mathrm{St} = \frac{2}{9}\frac{\tau_p}{\tau_f}, \tag{11}$$

where $\tau_p = a^2/\nu_0$ is the characteristic particle relaxation time and τ_f the characteristic time of the flow. In the present scaling $\tau_f = d^2/\nu_0$ such that the Stokes number becomes $\mathrm{St} = 2a^2/(9d^2)$.

To describe the motion of small particles in a viscous fluid the Maxey–Riley equation (Maxey and Riley, 1983) is frequently invoked. Keeping only the Stokes drag, added mass and the pressure gradient forces the simplification of the Maxey–Riley equation can be given in the form (Babiano, Cartwright, Piro, and Provenzale, 2000) (in the absence of gravity)

$$\ddot{\vec{y}} = \frac{1}{\rho + \frac{1}{2}} \left[-\frac{\rho}{\mathrm{St}} \left(\dot{\vec{y}} - \vec{u} \right) + \frac{3}{2} \frac{\mathrm{D}\vec{u}}{\mathrm{D}t} + \frac{\rho - 1}{\mathrm{Fr}^2} \vec{e}_g \right], \tag{12}$$

where $\vec{y}(t)$ is the location of the center of the spherical particle, $\mathrm{D}/\mathrm{D}t = \partial/\partial t + \vec{u} \cdot \nabla$ is the substantial derivative with respect to the fluid motion, $\mathrm{Fr} = \nu_0/\sqrt{gd^3}$ the Froude number and $\vec{e}_g$ the unit vector in the direction of gravity.

A more severe approximation is the so-called inertial equation (Haller and Sapsis, 2008), in which the sixth-order system (12) is reduced to a third-order system

$$\dot{\vec{y}} = \vec{u} - \left[\mathrm{St}\,(\rho - 1) \left(\frac{\mathrm{D}\vec{u}}{\mathrm{D}t} + \frac{\vec{e}_g}{\mathrm{Fr}^2} \right) \right]. \tag{13}$$

where the terms in the brackets cause a deviation of the particle's motion from that of the flow. In a solenoidal flow, a non-zero value of this term will by definition cause some degree of particle segregation and accumulation.

In the following sections an overview will be given of the results obtained within the JEREMI collaboration. Owing to the different approaches by which the problem has been tackled, the assumptions and simplifications made, in particular in the numerical models, vary to some degree. Therefore, deviations from the formulation given in this section will be briefly explained in the respective section.

3 Results

3.1 Experiments on PAS at the Tokyo University of Science (I. Ueno)

The heat transfer between the liquid bridge and the ambient gas can have a strong influence on the critical conditions for the onset of hydrothermal waves (Neitzel, Chang, Jankowski, and Mittelmann, 1993; Kamotani, Wang, Hatta, Wang, and Yoda, 2003; Ueno, Kawazoe, and Enomoto, 2009). Therefore, precise control of the ambient conditions is mandatory for comparable and accurate experiments on the critical flow conditions and on the formation of PAS. In order to take into account the effect of the heat transfer between the liquid bridge and the ambient gas flow, we employ a coaxial shield to realize forced upward or downward flow at various flow rates around the liquid bridge.

3.1.1 Experimental setup

The apparatus is described in Fig. 2. Frame (a) indicates a cross-sectional view from the side, while (b) shows a schematic of the top view to explain the spatial arrangement between the liquid bridge, the shield, the infrared (IR) camera (not shown) and the high-speed camera for the side view. The system is essentially the same as employed by Ueno, Tanaka, and Kawamura (2003). The height d and radius R of the liquid bridge are 1.6 mm and 2.5 mm respectively. The aspect ratio is $\Gamma = 0.64$. The volume ratio is $V/V_0 = 1$ ($V_0 = \pi R^2 d$). Under these conditions line-like PAS (SL-PAS) with azimuthal wave number $m = 3$ can robustly be realized in the case when the liquid bridge is open to the ambient atmosphere (Tanaka, Kawamura, Ueno, and Schwabe, 2006). We employ n-decane ($\mathrm{Pr} = 15$) and 2-cSt silicone oil ($\mathrm{Pr} = 28.1$) as the test fluids. Their physical properties are listed in Table 1.

The top rod is made of sapphire enabling an axial observation of the flow field in the liquid bridge. The bottom rod is made of aluminum. The top rod is electrically heated to realize a designated temperature T_h and the bottom rod is cooled by

Table 1: Physical properties of n-decane at 30 °C and 2-cSt silicone oil at 25 °C.

	n-decane	2-cSt silicone oil
ρ (kg/m^3)	7.31×10^2	8.73×10^2
ν (m^2/s)	1.27×10^{-6}	2.0×10^{-6}
κ (m^2/s)	8.45×10^{-8}	7.12×10^{-8}
σ (N/m)	23.9×10^{-3}	18.3×10^{-3}
γ (N/m K)	11.8×10^{-5}	7.15×10^{-5}
Pr	15	28.1

water to maintain the temperature at T_c so as to realize the designated temperature difference $\Delta T = T_h - T_c$. The temperatures of both rods are measured by thermocouples. The disk of the bottom rod has a sharp edge to prevent leakage of the test liquids. We observe PAS from the top and from the side by using two high-speed cameras, and measure the surface-temperature distribution using an infrared cam-

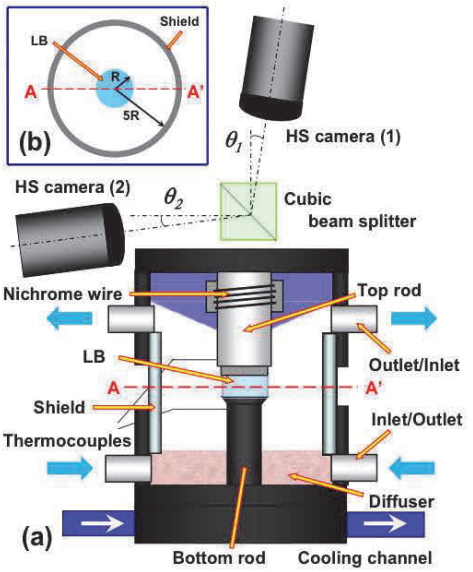

Figure 2: (a) Schematic of the cross-sectional view of the experimental apparatus in a side view and (b) in a top view showing the arrangement of the liquid bridge, the shield and the high-speed cameras.

era simultaneously as shown in Fig. 2. This way the spatio-temporal correlation between PAS and the hydrothermal wave can be measured. We confirm the validity of our experimental setup by making a comparison with the case of n-decane by Schwabe, Mizev, Udhayasankar, and Tanaka (2007). The whole series of experiments is conducted under the conditions where the hydrothermal wave is traveling, and not standing. Since the high-speed camera for the side view and the IR camera are located at $\Delta\varphi = \pi/2$ apart, the signals detected by both devices involve a constant phase shift of $\pi/2$. In the present study, we compare both signals after matching the phase as if both cameras were located at the same azimuthal angle.

In order to better control the heat transfer between the liquid bridge and the ambient gas flow, we employ a coaxial shield to realize forced upward or downward flow at various flow rates in the ambient gas region between the liquid bridge and the shield. The flow condition of the ambient gas in the external shield is characterized by an average velocity $U_{\mathrm{avg}} = Q/\pi(R_{\mathrm{ES}}^2 - R^2)$ and the Reynolds number $\mathrm{Re}_{\mathrm{amb}} = U_{\mathrm{avg}}\tilde{d}/\nu_{\mathrm{amb}}$, where Q is the controlled flow rate in the external shield, R_{ES} the radius of the external shield, $\tilde{d} = 2(R_{\mathrm{ES}} - R)$ is the hydraulic diameter of the anular channel part of which is used as a diffusor (see Fig. 2), and ν_{amb} the kinematic viscosity of the ambient gas. It is noted that $\mathrm{Re}_{\mathrm{amb}}$ is taken positive in the case of upward flow, conversely $\mathrm{Re}_{\mathrm{amb}}$ is negative in the case of downward one. The shield is made of Pyrex® glass. In the present study, we fix R_{ES} at 12.5 mm, and the thickness of the shield is 1.5 mm. The external shield has a tiny hole to insert a fine thermocouple through the shield to measure the temperature of the ambient gas. The ambient gas temperature is measured in the air gap along a radial ray at the mid-height of the liquid bridge in increments of 0.1 mm.

The heat-transfer effect between the liquid and the ambient gas is characterized by the Biot number

$$\mathrm{Bi} = -\frac{\lambda_{\mathrm{amb}}}{\lambda}\frac{(\partial T/\partial r)_{r=R}\, d}{T_{z=0} - T_{\mathrm{sh}}}, \tag{14}$$

where λ and λ_{amb} represent the thermal conductivities of the test fluids of the liquid bridge and the ambient gas, respectively, and T_{sh} is the wall temperature of the external shield. The surface temperature of the liquid bridge is measured by the IR camera through the external shield and ambient gas. To that end a small opening is cut out from the external shield and replaced by a small window of zinc selenide (ZnSe). The height, width and thickness of the window are of 22 mm, 7 mm and 1.5 mm, respectively. Owing to its small size the resulting non-uniformity of the curvature of the internal wall and the thermal non-uniformity have only a little effect (a few percent) on the critical Marangoni number as well as on the Biot number.

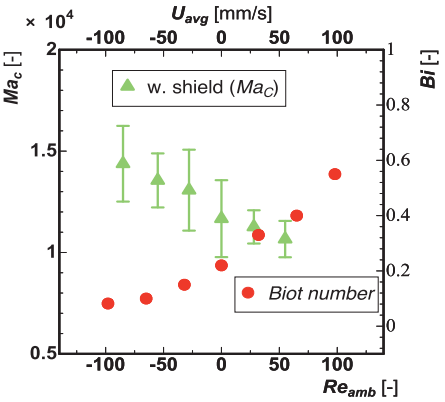

Figure 3: Critical Marangoni number (triangles) and Biot number (dots) as function of the ambient-gas Reynolds number.

To visualize the convection in the liquid bridge and to observe PAS, gold-coated acrylic particles of diameter 15 μm ($a = 7.5\,\mu$m) and density $\rho_p = 1770\,\mathrm{kg/m^3}$ are suspended in the liquid. For the 2 cSt silicone oil the particle Stokes number evaluates to $\mathrm{St} = (2/9)\,a^2/d^2 = 0.99 \times 10^{-5} \approx 10^{-5}$ if the viscous diffusion time d^2/ν is used for the time scale τ_f of the flow (aspect ratio $\Gamma = 0.64$). In fact, the period of oscillation of a hydrothermal wave under the conditions of line-like PAS (SL-1) is of the same order of magnitude $O(d^2/\nu)$ (Tanaka, Kawamura, Ueno, and Schwabe, 2006). The motion of the particles is observed through the transparent top sapphire disk by use of two high-speed cameras and a cubic beam splitter placed above the top disk. This system enables reconstruction of three-dimensional particle trajectories inside the liquid bridge via three-dimensional particle tracking velocimetry (3D-PTV). The details of the experimental procedures are described in Nishimura, Ueno, Nishino, and Kawamura (2005) and Abe, Ueno, and Kawamura (2009).

3.1.2 Measurements

Critical onset Here we report the results obtained for 2-cSt silicone oil as the test liquid. In a first step the critical Marangoni number $\mathrm{Ma}_c = \mathrm{Re}_c\mathrm{Pr}$ is determined as a function of the Reynolds number for the ambient gas flow $\mathrm{Re}_{\mathrm{amb}}$. Figure 3 shows the average value $\mathrm{Ma}_c(\mathrm{Re}_{\mathrm{amb}})$ obtained from five independent realizations along with the maximum and minimum of the measured values (shown as error bars). The critical Marangoni number Ma_c slightly decreases with increasing $\mathrm{Re}_{\mathrm{amb}}$ as was also observed by Ueno, Kawazoe, and Enomoto (2009). In case of upward-directed forced flow towards the hot disk ($U_{\mathrm{avg}} \geq 0$), the flow in the liquid is slightly

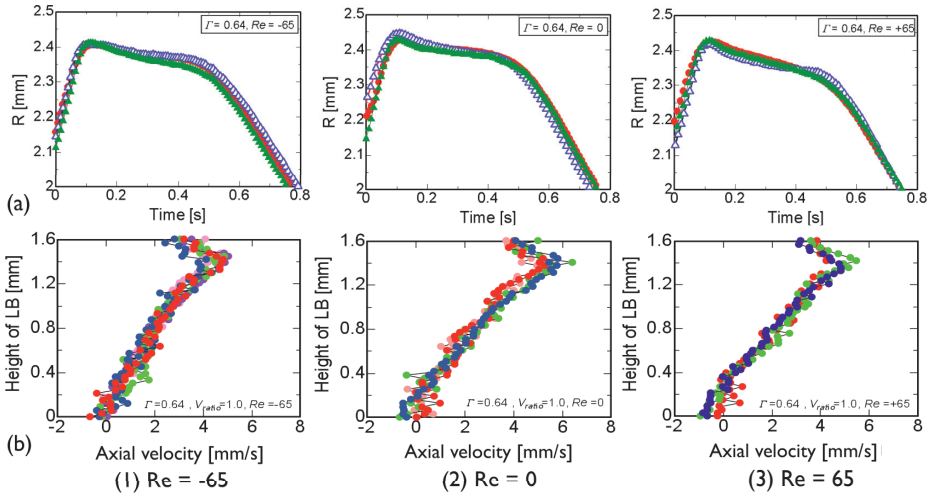

Figure 4: Representative particle trajectories near the free surface of the liquid bridge for $\varepsilon = 0.5$ and ambient-gas Reynolds numbers of $\mathrm{Re}_{\mathrm{amb}} = -0.65$ (1), 0 (2), and 0.65 (3).

destabilized. When the forced flow is directed downward towards the cold disk ($U_{\mathrm{avg}} < 0$), on the other hand, the axisymmetric basic flow in the liquid bridge is stabilized if the magnitude of the gas velocity is increased. The Biot number Bi evaluated under the condition of flow transition exhibits the opposite trend, i.e., Bi monotonically increases as $\mathrm{Re}_{\mathrm{amb}}$ is increased. This trend is opposite to the one found by Smith and Davis (1983) for the onset of hydrothermal waves in the return flow of a liquid layer.

Particle motion in the absence of PAS To investigate the effect of the ambient gas flow on the particle motion we have measured four randomly selected particle trajectories for three different ambient Reynolds numbers. In each case we considered a traveling hydrothermal wave at a Marangoni number 50% above its critical value, i.e. at $\varepsilon = (\mathrm{Ma} - \mathrm{Ma}_c)/\mathrm{Ma}_c = 0.5$. These Marangoni numbers are less than the Marangoni numbers for which line-like PAS can be observed. The trajectories obtained by 3D-PTV are shown near the free surface in Fig. 4.

In the upper figures (a) of Fig. 4 the radial coordinates of the particles are plotted as a function of time. In (b) the axial velocity of the particles is shown, during the time they spent near the free surface, as functions of their vertical position. The individual trajectories have been time-shifted such that the instant of closest

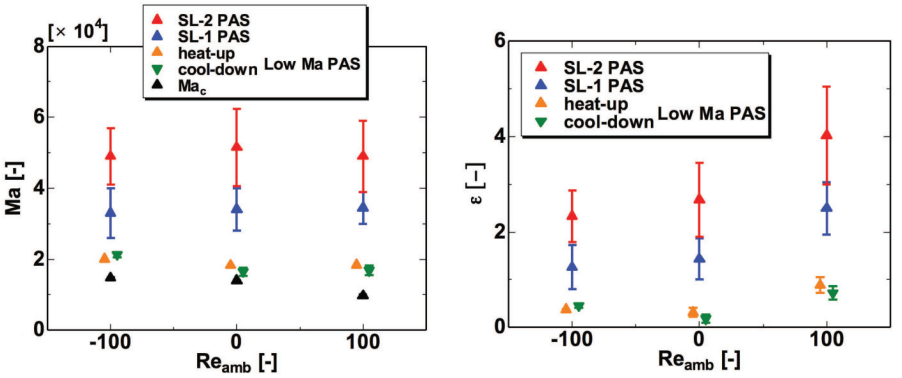

(a) (b)

Figure 5: Existence ranges in terms of Ma (a) and ε (b) for different line-like PAS: SL-1 (red), SL-2 (blue), and low-Ma PAS (orange/green) for different gas-flow conditions. The critical Marangoni number is shown in black.

approach to the free surface occurs at $t = 0.1$ s.

We find that the particle trajectories do not significantly depend on the gas flow. Near the hot wall they all travel toward the free surface ($0 < t < 0.1$) and approach it very closely ($t \approx 0.1$). Thereafter, they move near the free surface toward the cold wall ($0.1 < t < 0.5$) with a very weak negative radial velocity component. After $t = 0.5$ the radially inward motion becomes faster and the particles return to the bulk in the cold half of the liquid bridge. Finally, they return to the hot wall near the axis (not shown). The particles' velocity profiles in the axial direction near the free surface (frames (b) of Fig. 4) indicate that the particle motion in z direction is hardly affected by the ambient gas flow. The particles are accelerated near the hot-end wall and decelerated over most part of the liquid height when they move towards the cold end wall. Such behavior has also been observed for the particles on PAS (Niigaki and Ueno, 2012).

Existence range of PAS and correlation with the temperature field Figure 5 shows the existence ranges of line-like PAS of type SL-1 and SL-2 for different gas-flow conditions for the Marangoni number (a) and for the reduced Marangoni number ε (b). The onset conditions are determined by evaluation of the particle pattern by the naked eye. For slightly supercritical flow we find a small window in Ma for which line-like PAS exists. This narrow existence window follows the trend of the critical Marangoni number which decreases with $\mathrm{Re}_{\mathrm{amb}}$. The figure indicates that the SL-PAS regimes emerge for different ranges of the reduced Marangoni

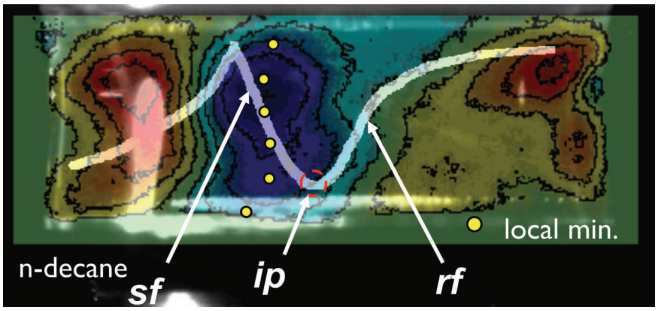

(a)

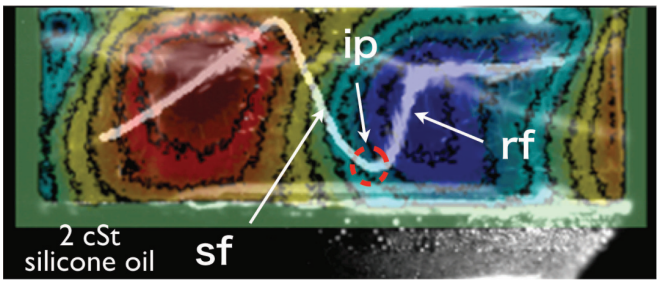

(b)

Figure 6: Spatial correlations between PAS and the surface-temperature deviation for liquid bridges of $V/V_0 = 1.0$ under $\mathrm{Re}_{\mathrm{amb}} = 0$ in the cases of n-decane (a) and 2-cSt silicone oil (b). The experimental conditions for n-decane are $(\Delta T, \mathrm{Ma}) = (19.8, 4.8 \times 10^4)$. For 2-cSt silicone oil $(\Delta T, \mathrm{Ma}) = (42.0, 4.0 \times 10^4)$. In both cases the wave travels from the right to the left.

number; the existence ranges in terms of ε are increasing with $\mathrm{Re}_{\mathrm{amb}}$.

For n-decane Schwabe, Mizev, Udhayasankar, and Tanaka (2007) have suggested a strong correlation between PAS with $m = 3$ and the flow and temperature field in their Fig. 9. Those parts of the particle trajectory which are close to the free surface and those parts which are in the bulk have been denoted 'sf' (surface flow) and 'rf' (return flow). They assigned a particular importance to the point of the trajectory at which the particle leaves the free surface and turns into the bulk. Even though this point which is denoted 'ip' (injection point) is not precisely defined in the experiments, it is similar to the release point of Hofmann and Kuhlmann (2011) which is exactly defined within their particle motion model.

In order to establish such a correlation for 2-cSt silicone oil we first carried out a series of experiments with n-decane to validate our experimental system (Fig. 6a). The result for 2-cSt silicone oil is shown in Fig. 6b. Both spatial correlations

between PAS and the surface-temperature deviation have been obtained for $V/V_0 = 1.0$ and $\mathrm{Re}_{\mathrm{amb}} = 0$. In both sub-figures the hydrothermal wave travels from right to left. The net traveling direction in the azimuthal direction of the particles on PAS is known to be opposite to that of the hydrothermal wave (Tanaka, Kawamura, Ueno, and Schwabe, 2006). Therefore, the particles on PAS travel from left to right in Fig. 6.

The correlation between PAS and the temperature field (and hence also the flow field) differs for n-decane and 2-cSt silicone oil. While in both cases PAS is very similar and the particles reach close to the free surface (corresponding to maximum of the projected trajectories in Fig. 6) near the hot-end wall, this arrival at the free surface occurs in the region of the *cold*-temperature surface spot for n-decane (a), but in the region of the *hot*-temperature surface spot for 2-cSt silicone oil (b). The result for n-decane agrees well with the results by Schwabe, Mizev, Udhayasankar, and Tanaka (2007) in spite of the different experimental setups. The phase shift of PAS for the 2-cSt silicone oil is somewhat unexpected. This deviation occurs for all volume ratios in the range $0.9 \leq V/V_0 \leq 1.0$. This phenomenon may possibly be explained by a different density ratio ρ due to the different densities of the liquids (see table 1). The shape of PAS does not depend very much on ρ in the model of Muldoon and Kuhlmann (2013a). However, PAS lags behind the hydrothermal wave the larger $\rho > 1$ is. This is consistent with the experimental result for which $\rho = 2.42$ (30°C) and 2.03 (25°C) for n-decane and 2-cSt silicone oil, respectively.

3.2 Particle-motion attractors by dissipation near the free surface (H. C. Kuhlmann, R. V. Mukin, F. H. Muldoon)

The work of the Vienna group has focused on gaining an understanding of PAS: Why does PAS arise, what shapes can it take, how long is its formation time, and on which flow and particle properties does it depend? Once these question can be answered satisfactorily, reliable predictions become possible, e.g., for the planned JEREMI experiment.

In the following we consider a three-dimensional traveling hydrothermal wave for $\Gamma = 0.66$, $\mathrm{Pr} = 4$ and $\mathrm{Bi} = 0$. Streamlines of the incompressible flow in the liquid bridge are either chaotic or regular (Hofmann and Kuhlmann, 2011; Mukin and Kuhlmann, 2013). This elementary property of volume-preserving flows is of eminent importance for mixing (Ottino, 1989). A regular streamline winds on a closed torus. Such tori, called KAM tori, arise as densely nested sets, each set hosting a central closed streamline. Since the velocity is always tangent to a KAM torus, fluid inside of a torus remains completely separated from the fluid outside of it. Since the KAM tori are not easy to find for the three-dimensional time-dependent flow in the laboratory frame of reference, it is useful to consider the hydrothermal

Figure 7: Dominating KAM tori (not all tori are shown) for Re = 2600: T_3^3 (blue), the core T_{core} (red) and T_{1a}^9 (yellow). The circle indicates the free surface.

wave in a co-rotating frame of reference in which the flow is steady. Fig. 7 shows some (but not all) of the most important KAM tori for Re = 2600. Most streamlines inside of the tori shown are regular, winding on nested tori. The streamlines outside of the separating KAM tori (in the empty space of Fig. 7) are chaotic and make the so-called chaotic sea.

Note that line-like PAS as visible in Fig. 1b is neither a closed trajectory for fluid elements nor for particles. The central closed streamline (not shown) inside of the blue KAM torus in Fig. 7, however, resembles line-like PAS. This observation indicates the importance for PAS of the central closed streamlines inside of the KAM tori.

In order to model the particle motion we summarize the experimental evidence. (I) PAS formation from a disordered particle arrangement can be very rapid. Therefore, the particle motion must be subject to a *strong* dissipative effect. *Dissipative effect* is used here in the sense of classical mechanics to indicate that the Liouville theorem is violated and the flux in phase space of a particle is non-solenoidal (Schuster, 1984). (II) Neutrally-buoyant particles accumulate the fastest (Schwabe, Mizev, Udhayasankar, and Tanaka, 2007). Therefore, the major dissipative effect does not depend on the density mismatch between particles and liquid. (III) Tanaka, Kawamura, Ueno, and Schwabe (2006) have shown that, apart from line-like PAS, a toroidal core of particles exists (Fig. 1b) within which the particles move nearly as perfect tracers. The core of particles is very similar to the KAM torus (red in Fig. 7) about which the other tori wind. Apparently, the dissipative effect on the core particles is negligible. (IV) Particles on line-like PAS move extremely close to the free surface (Tanaka, Kawamura, Ueno, and Schwabe, 2006). (V) The existence of PAS and its formation time depends on the particle size (Schwabe, Mizev,

Udhayasankar, and Tanaka, 2007) which thus is an important parameter. (VI) At low supercritical Marangoni numbers only a particle depletion zone (Fig. 1a) exists in the center of the liquid bridge (Ueno, Ono, Nagano, Tanaka, and Kawamura, 2000; Kawamura, Ueno, and Ishikawa, 2002; Ueno, Tanaka, and Kawamura, 2003) (see also Muldoon and Kuhlmann, 2013a). The particles which are expelled from this central region are those which approach the free surface most closely.

The sum of these experimental results gives strong evidence for a dissipative effect located in a thin layer below the free surface whose thickness is related to the particle size. This is not surprising given the extreme streamline crowding with rapid flow and high shear in the free-surface boundary layer. An obvious finite-size effect is the restriction of the radial motion of the particles as they approach the free surface. With the precise details of the particle–free-surface interaction being unknown, the restricted motion is modeled by an inelastic wall for the center of the particle located at $R^* = R - \Delta$ (particle–free-surface interaction length) (Hofmann and Kuhlmann (2011); Kuhlmann and Muldoon (2012b); Muldoon and Kuhlmann (2013a); Mukin and Kuhlmann (2013)), where $\Delta(a)$ is closely related to the particle radius a. To isolate the dissipative free-surface effect on the particle motion from volume dissipation due to inertial effects we assume perfect-tracer motion in the bulk, i.e. $\rho = 1$.

If a KAM torus intersects R^*, particles moving on quasi-periodic regular orbits are affected by the hard-wall interaction. As a result they are mapped on R^* from one regular streamline to another. Hofmann and Kuhlmann (2011) have shown how this mapping leads to a limit cycle when the central closed streamline of a system of nested KAM tori slightly intersects R^*. The limit cycle for the particle motion represents line-like PAS (also called SL-1-PAS). When the maximum KAM torus which separates a set of regular streamlines from the chaotic sea intersects R^* but the central closed streamline does not, then the attractor for the particle motion is a tube which is tangent to R^*. This is called tubular PAS. The particles inside tubular PAS, which is a visualization of a particular KAM torus, are not affected by the hard wall. However, particles from that part of the regular region which is outside of the tangent tube are attracted to the tangent tube. In an experiment tubular PAS would appear as a widened PAS with an enhanced edge. A numerical result is shown in Fig. 8a.

Other types of attractors also exist in this model for the particle motion. If no KAM torus intersects R^* only chaotic streamlines are mapped among each other by way of the hard-wall model. Due to the mapping, those streamlines which originate from the annular region $[R^*, R]$ cannot be re-populated by particles. Therefore, these streamlines become depleted. This effect leads to a characteristic depletion zone near the axis, which resembles a triangle for the flow with $m = 3$ at $\Gamma =$

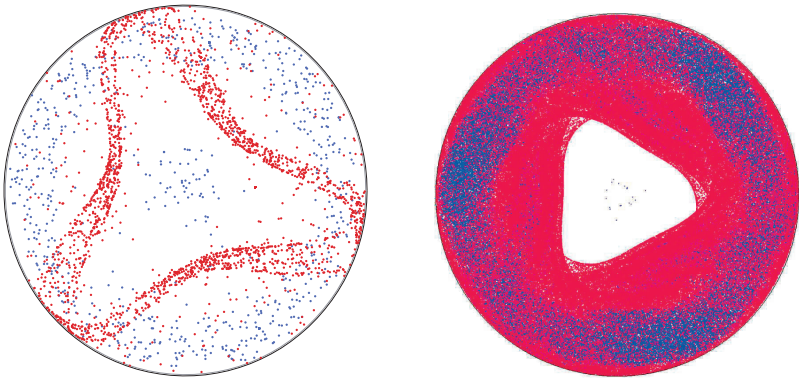

(a) Tubular PAS for the Navier–Stokes flow from 6000 initially random particles after $t = 5$ for $\Delta = 0.01$.

(b) Strange PAS for $\Delta = 0.0067$ using the analytical model of Muldoon and Kuhlmann (2013a), Physica D. Compare with Fig. 1a.

Figure 8: PAS for $\mathrm{Re} = 1800$ using the perfect-tracer model with the addition of the particle–free-surface and particle-wall interaction model. Red indicates particles that have interacted with the free surface at least once, blue those that have never interacted.

0.66 (Fig. 1a). This form of PAS is called strange PAS, because the attractor for the particles which are removed from the central region is a strange attractor in the framework of the hard-wall model (Fig. 8b, see also Muldoon and Kuhlmann, 2013a). The depletion triangle is a very robust experimental feature (see e.g. Ueno, Tanaka, and Kawamura, 2003) and thus a strong argument for the hard-wall model.

The detailed mechanisms and other forms of PAS are beyond the scope of the present paper. The reader is referred to Hofmann and Kuhlmann (2011); Kuhlmann and Muldoon (2012b); Muldoon and Kuhlmann (2013a); Mukin and Kuhlmann (2013) for comprehensive in-depth results and explanations. One remarkable property of the hard-wall model is that particles initially on streamlines of the chaotic sea can drain entirely to line-like PAS. This effect makes PAS clearly visible in the experiments. In addition to line-like PAS only those particles remain suspended which move on KAM tori which do not interact with the free surface, e.g., the particles in the toroidal core T_{core} (Fig. 1b and red in Fig. 7).

The hard-wall model is capable of reproducing all important features observed in the experiments: line-like PAS, the depletion zone and the toroidal core. Moreover, details of the particle dynamics are predicted (Muldoon and Kuhlmann, 2013a; Mukin and Kuhlmann, 2013) which can be used to further validate the model or to refine, e.g., the particle–free-surface interaction model. The inclusion of particle

inertia and buoyancy (although typically of minor importance, see Kuhlmann and Muldoon, 2012b) does not change the general type of the problem: Owing to the one-way coupling of the particle to a given space- and time-periodic flow its motion is governed by an *autonomous* dynamical system in the co-moving frame of reference. Within the context of a model based on the Maxey–Riley equation, such as (12), PAS is a *single-particle phenomenon* and can thus be completely understood in the framework of dissipative structures of dynamical systems. Therefore, line-like PAS is the attraction, under a stationary flow, of points in the particle phase space to a stable limit cycle from its basin of attraction. It is not required and would, in fact, be misleading to interpret PAS in terms of further theories which may not be applicable to the present dynamical-system modeling (see e.g. Kuhlmann and Muldoon, 2012a).

To investigate PAS for higher-Prandtl-number liquids which are to be investigated in the JEREMI experiment, further studies are required. A complication is the extremely high numerical resolution required to resolve the KAM structures near the free surface for such high-Prandtl-number liquids. The investigations are further complicated by numerical errors such as the truncation error of the majority of time-integration schemes for the particle motion. Another error results from the creation from a discrete flow field of a continuous interpolant which in general is not solenoidal in a strong (pointwise) sense. All these numerical errors are sources of dissipation. Such numerical dissipation causes deviations of the motion of neutrally-buoyant particles from that of the solenoidal flow and leads to some form of particle accumulation. The numerical-error-induced structures can be very similar both in shape and formation time (Muldoon and Kuhlmann, 2013b) to experimentally observed PAS, PAS resulting from the inelastic hard-wall model and PAS resulting from particle inertia.

3.3 Organization of small inertial particles into dynamic coherent structures by phase locking (D. O. Pushkin, D. E. Melnikov, V. M. Shevtsova)

The work of the Brussels group includes both experimental and theoretical studies. It has focused on two main areas: (1) gaining a fundamental understanding of how and when the dissipative interactions between the particles and the fluid flow may lead to a formation of one-dimensional particle accumulation, and (2) developing a reliable code for simulating particle dynamics in realistic flows and under conditions realized in the experiments of Schwabe, Tanaka, Mizev, and Kawamura (2006), Tanaka, Kawamura, Ueno, and Schwabe (2006) and Kawamura, Nishino, Matsumoto, and Ueno (2012).

In order to explain the mechanism of PAS formation we have postulated an analytical model of a steady cylindrical flow with a superimposed azimuthally traveling

wave (Pushkin, Melnikov, and Shevtsova, 2011). This model is generic, as similar flow patterns often develop due to hydrothermal instabilities in cylindrically symmetric systems (see e.g. Kuhlmann, 1999; Shevtsova, Melnikov, and Legros, 2001). On the other hand this approach allows circumventing the problem of numerical interpolation of the flow from the grid. Next, assuming weightlessness, a simple dissipative model of particle motion was postulated by assuming that the motion is governed by the inertial term in the Maxey–Riley equation, dominant in most situations except for the case of strictly density-matched particles. Later this restriction was relaxed by accounting for the remaining terms of the Maxey–Riley equation with no significant change in the results.

It was found that this generic model leads to a formation of particle accumulation structures having both structure and dynamics analogous to PAS. The model allows using the dynamical systems theory and establishing a correspondence between PAS and fixed points of the equatorial Poincaré section (Pushkin, Melnikov, and Shevtsova, 2011). Similar to the PAS observed in the experiments and numerical simulations by Melnikov, Pushkin, and Shevtsova (2011), the PAS formation occurs only for a special choice of the system parameters; in particular it occurs only when the frequency of the particle turnover motion and the angular frequency of the wave in the Lagrangian system of the particle are commensurate. This *resonance condition* for PAS had first been noted by Schwabe, Mizev, Udhayasankar, and Tanaka (2007). In order to explain this observation and to account for the robustness of the features of PAS with respect to the dissipative interaction, the Brussels group put forward the phase-locking theory of PAS formation.

In this theory, PAS formation is attributed to synchronization (Pikovsky, Rosenblum, and Kurths, 2003) of the particle turnover motion with the wave due to a weak, repeated dissipative interaction with the traveling wave. In this process the particle's turnover frequency becomes locked to a rational multiple of the frequency of the hydrothermal wave. The arising spirals rotating with the angular frequency of the wave are then akin to the phenomenon of the Mexican wave that propagates in a stadium due to synchronized motions of the spectators. A particle, being a chaotic oscillator with a wide-band frequency spectrum imposed by the thermocapillary flow, experiences periodic inertial interactions with the periodic azimuthal flow (hydrothermal wave). It moves the particle forth and back in the plane perpendicular to its turnover motion with a frequency of the wave Ω "seen" by the moving particle in the corresponding Lagrangian frame of reference. As time passes, the periodic pushing–pulling will have a cumulative effect resulting in an adjustment of the particle's orbit of the turnover motion. Consequently, its azimuthal velocity also changes and the particle will experience the pushing–pulling action with a different frequency and amplitude (Pushkin, Melnikov, and Shevtsova, 2011).

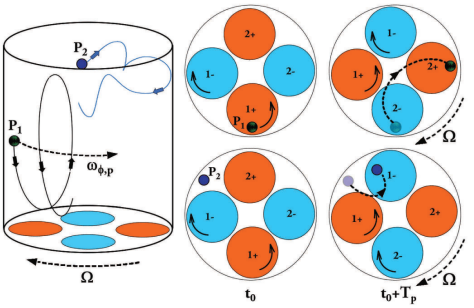

Figure 9: Sketch of the mechanism of PAS formation. A phase-locked with the wave P_1 and quasi-periodic P_2 particles are shown. A hydrothermal wave with mode $m = 2$ is schematically pictured. The spots at the cross section represent 2 pairs of vortices numbered $1+, 2+$ and $1-, 2-$, where the number marks the vortex and the $+$ or $-$ signs show positive and negative vorticity. The direction of azimuthal velocity is indicated by arrows, projections of the trajectories of the particles on the equatorial plane within one turnover period T_p of the periodic particle P_1 are shown by dashed arrows in the direction of their motion.

It takes time to synchronize a particle, and as was shown, the PAS formation time for the very small particles grows as a^{-n}, where experimental values of n vary between 1.5 and 3 (Schwabe, Mizev, Udhayasankar, and Tanaka, 2007) and $n = 2$ having been predicted numerically by the model of the Brussels group (Pushkin, Melnikov, and Shevtsova, 2011, 2012). While the particle's orbit slowly changes with time due to non-conservative forces, it can approach a resonance and then remain trapped there even under further action of the non-conservative forces. The locking mechanism is able to preserve the resonance once attained.

Figure 9 shows a sketch of the mechanism of PAS formation. Two particles are marked: P_1 belonging to a PAS, and P_2 on the torus. The hydrothermal wave rotates clock-wise with a constant frequency Ω (frequency with which a vortex, e.g., $1+$, makes 2π), while the P_1 particle drifts in the opposite direction with a time-average frequency $\omega_{\phi,p}$. T_p is the turnover period of the particle P_1, i.e., the time between two consecutive crossings of the equatorial (at the mid-height of the liquid bridge) plane. After T_p, the PAS particle comes exactly to the same location on the paired vortex $2+$, i.e., P_1 and the wave cover the total angle of $2\pi/m$

$$T_p\left(\omega_{\phi,p} + \Omega\right) = \frac{2\pi}{m}. \tag{15}$$

Since the two paired vortices are equivalent in terms of the phase of the wave, the P_1 particles and the wave are phase-locked. Equation (15) does not hold for the P_2

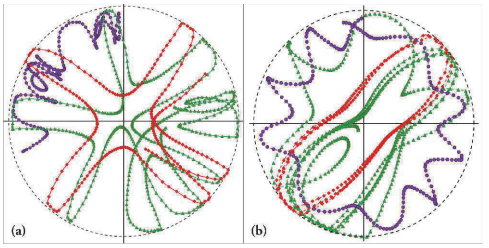

Figure 10: Experimental trajectories of three particles reconstructed in laboratory (a) and rotating (b) frames of reference. The dashed circle is an approximate location of the liquid–air interface.

particle, and both its turnover period and frequency of its mean azimuthal drift are not time-constant in general.

When a synchronization occurs due to interactions with the environment, one observes a significant decrease of the number of effective degrees of freedom of a whole system, and this is what the particles on the periodic orbits are undergoing. Trajectories constituting the PAS line are *almost* identical, they repeat themselves after each particle's turnover period T_p. Many particles performing the identical motion create an essentially one-dimensional thin line structure, whose shape does not change much with time.

In order to address the mechanism of PAS formation delineated above, we performed a set of ground experiments in a non-isothermal liquid bridge made of n-decane with a counter gravity imposed temperature gradient, in which the liquid volume was maintained constant at the value close to the volume of the cylinder. The experimental setup has been designed and built by D. Schwabe and is described in Schwabe, Tanaka, Mizev, and Kawamura (2006); Schwabe, Mizev, Udhayasankar, and Tanaka (2007). The study was done for a liquid bridge of 3 mm both in radius and height using spherical particles about 8 % denser than the liquid with a broad distribution in size (approximately between 20 and 100 microns in diameter, therefore yielding values of the Stokes number St between 2.4×10^{-6} and 6×10^{-5}).

It has been found that the particles, with the exception of those that sediment, either converge to a periodic or a quasi-periodic stable resonant orbit or exhibit intermittent dynamics during which the trajectory is nearly periodic with temporary interruption. We call these intermittent orbits quasi-stable periodic orbits. An example of the three types of experimental trajectories is given in Fig. 10. They are reconstructed in the laboratory (Fig. 10a) and in a rotating frame of reference (Fig. 10b). The latter rotates azimuthally together with the hydrothermal wave, in the same di-

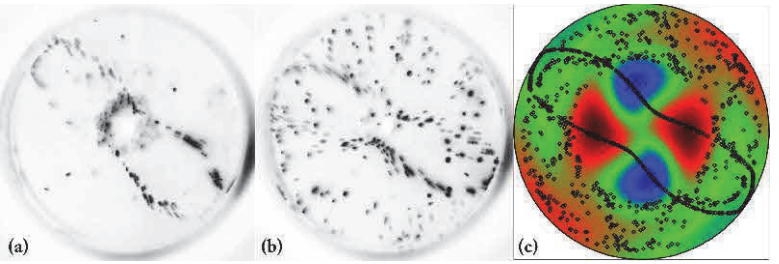

Figure 11: Snapshots of distributions of particles observed in experiments at $\Delta T = 9.29K$ (a), $\Delta T = 9.75K$ (b) and simulations performed at $\Delta T = 9K$ for particles with $St = 6 \times 10^{-5}$ (c). Locations of particles are marked by black symbols, colors represent temperature disturbances at the horizontal cross-section. High and low temperature are shown by red and blue color respectively.

rection and with the same angular velocity. In Fig. 10, the red, magenta and green symbols represent periodic, quasi-periodic and quasi-stable periodic trajectories, respectively. The three types of motion were sometimes observed simultaneously. In the rotating frame of reference, the periodic orbits and the PAS line coincide.

Those particles that move along the periodic orbits were found to drift azimuthally opposite to the direction of propagation of the hydrothermal wave. In turn, the quasi-periodic particles move in the same direction as the wave but with a smaller angular velocity than that of the wave.

When observing a large amount of periodic particles the phenomenon of PAS occurs, creating an illusion of a thin closed rigid structure rotating azimuthally with a constant velocity (examples of PAS are given in Fig. 11a,b). In turn, many quasi-periodic orbits form a torus. We have noticed that PAS is constituted of relatively small particles while the torus is populated by the large ones. The accumulation structures in Fig. 11 are called SL-1 (spiral loop) PAS, but different stable resonant orbits, e.g. SL-2 PAS, may appear (Tanaka, Kawamura, Ueno, and Schwabe, 2006).

The quasi-stable periodic orbits consist of alternating time spans of periodic and quasi-periodic motion, resembling the periodic (red) and quasi-periodic orbits (magenta), respectively. When the quasi-stable particle motion changes from periodic to quasi-periodic, or vice versa, the direction of the azimuthal drift is inverted. The difference between the red periodic and the green quasi-stable periodic orbits is best seen in the rotating frame of reference in Fig. 10b. While the former is symmetric and centered with respect to the symmetry axis of the liquid bridge, the latter, when in the periodic phase, is not. The quasi-stable periodic particles are not synchronized among each other, i.e., each of them enters and leaves a periodic

window independent from the others. The presence of these particles in the flow makes PAS look fuzzy, as shown in Fig. 11b. The experimental results in Figs. 11a and b were obtained for the same particles but at different values of the imposed ΔT. Since the flow depends sensitively on the temperature difference, it effects the dynamics of the particle motion. By variation of ΔT we were able to observe either a thin PAS line together with a very weak torus (Fig. 11a) or a scattered PAS line accompanied by a torus comprising of a large amount of particles at a larger value of ΔT (Fig. 11b).

The appearance of the three types of trajectories of particles is a result of the phase-locking process. Although the transition to the synchronized state in a chaotic system is always smeared, some particles with *suitable* inertial properties phase lock with the wave ending up on periodic orbits, whereas for the others it either never happens (quasi-periodic orbits) or is a temporary event on finite-time intervals only (quasi-stable periodic orbits). The parameter region in the phase plane, where synchronization is possible, is called *Arnold tongue* (Arnold, 1983; Pikovsky, Rosenblum, and Kurths, 2003). Particles on quasi-stable periodic orbits are associated with the border of Arnold tongue, i.e., where *complete* phase-locking is impossible *phase slip* occurs.

Computer modeling performed for the same experimental conditions shows that the shape of PAS reflects the structure of the supercritical flow. If one thinks of PAS as an epicycloid with m vertices, then m is prescribed by the flow as is shown in Fig. 11c in which the deviation of the temperature field from its azimuthally average is shown. The supercritical thermocapillary flow is characterized by wave number $m = 2$, and therefore the PAS has two vertices.

3.4 General properties and variety of one-dimensional solid particle attractors in spatio-temporal periodic flows (M. Lappa)

The investigations at Telespazio on PAS have concentrated on existing experimental systems (Lappa, Savino, and Monti, 2000; Lappa, 2003; Lappa and Savino, 2002; Lappa, 2005). In particular, an understanding of the sensitivity and robustness of the PAS phenomenon against changes of the effective setting used for the experiments has been developed. The factors considered are the geometry, the kinematic boundary conditions and the nature of the external forces which affect the fluid and particle motion (surface-tension gradients, gravitational or vibrational forces). The present section collects numerical results which have already been published. We provide a critical synthesis of the most interesting physical arguments, especially of those which are expected to be applicable to a vast range of other problems. For a more in-depth analysis the interested reader is referred to the original work.

For brevity, we consider only a Marangoni number twice the critical value, as PAS

can be observed experimentally most reliably for this condition. In particular, all examples shown in this section are for $\Gamma = 0.68,\ \mathrm{Pr} = 8,\ \mathrm{Ma} = 20600$ and $\mathrm{Bi} = 0$. The problem was initially investigated by Lappa (2013a) by numerical solution of the Navier-Stokes equations and energy equations coupled with (13) the explicit dissipative equation describing the flow on the slow manifold that governs the asymptotic behavior of inertial particles.

As PAS is an azimuthally periodic structure rotating with the phase velocity of the wave, the turn-over frequency (about the toroidal vortex core) of an individual particle of PAS must be correlated with the phase velocity of the hydrothermal wave. As described in other sections of this paper, two main theories are proposed to explain the focusing of particles on PAS. While Pushkin, Melnikov, and Shevtsova (2011) describe this process in terms of a phase locking mechanism, Muldoon and Kuhlmann (2013a) describe it in terms of a structural instability of an elliptic orbit of a KAM torus which is a topological feature of the flow.

At Telespazio it was decided to first consider the *phase-locking model* and analyze PAS in terms of particle axial vorticity. This has been achieved by replacing the particle turnover frequency with equivalent arguments on the particle angular spin, an alternate point of view that should be seen as a more spatial perspective, an application of what is generally regarded as *vorticity thinking* (Lappa, 2012). In practice, this new point of view originates from a simple model in which the axisymmetric basic flow can be represented by a pure azimuthal vorticity field, while the hydrothermal wave consists essentially of axial vorticity (see also Wanschura, Shevtsova, Kuhlmann, and Rath, 1995; Muldoon and Kuhlmann, 2013a). In this simplified picture the azimuthal and the axial vorticity represent the strength of the basic toroidal flow and that of the hydrothermal wave, respectively, the latter measuring the local rotation rate of the fluid about a vertical axis.

The numerical results, an example is shown in fig. 12, clearly demonstrate a certain relation between PAS and the vorticity $\vec{\zeta} = \nabla \times \vec{u}$ of the hydrothermal wave. In particular, we find that PAS tends to stay attached, for most of its azimuthal extension, to those isosurfaces of the axial vorticity ζ_z which equals twice the rotation rate $\Omega_{\mathrm{wave}} = 2\pi f/m$ of the hydrothermal wave (Lappa, 2013a), where f is the frequency of the hydrothermal wave measured at a generic point. As the local axial rotation rate of the fluid $\Omega_{\mathrm{fluid}} = \zeta_z/2$ is one half of the axial vorticity, this condition is equivalent to $\Omega_{\mathrm{fluid}} = \Omega_{\mathrm{wave}}$, which indicates that the basic ideas of Pushkin, Melnikov, and Shevtsova (2011) can be expanded/revisited via direct incorporation of relatively simple ideas of vorticity–wave interaction (see e.g. Rhines, 1975).

This strong geometric correlation still holds (Lappa, 2013a) for a thermocapillary annular pool with adiabatic bottom and heating from the outer cylinder and/or when additional vorticity is injected into these systems by rotating the top disk (liquid

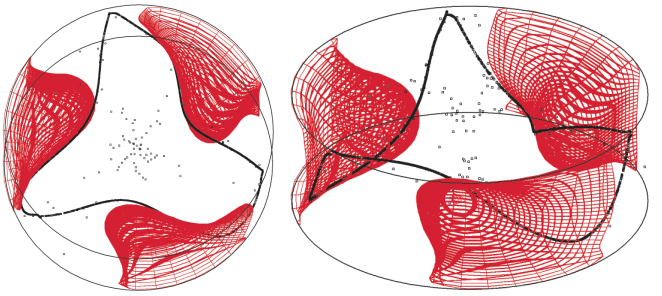

(a) (b)

Figure 12: Two different views of PAS (black line) together with iso-surfaces (red) of the local axial rotation rate of the fluid for $\Omega_{\text{fluid}} = 9$. The flow parameters are $\text{Pr} = 8$, $\Gamma = 0.64$, $\text{Ma} = 20600$, $m = 3$, $\Omega_{\text{wave}} = 8.92$. The hot disk is on the top and the cold disk on the bottom. The cylindrical free surface is adiabatic. The particle parameters are $\rho = 1.85$ and $\text{St} = 10^{-4}$.

bridge) or the outer cylindrical wall (annular pool). Remarkably, this property has been found to also apply to Rayleigh-Bénard convection in a cylinder when convection arises in form of at least one toroidal roll and a wave-disturbance traveling in the azimuthal direction; conditions that seem to be satisfied only for $\text{Pr} \simeq 1$ in a region of parameter space in which the so-called OS mode of the Busse balloon (Busse, 1978) occurs (Lappa, 2013b).

In pursuit of understanding realistic situations the work at Telespazio then shifted to the subject of identifying and quantifying effects which disturb the fundamental mechanisms supporting PAS. In this respect, additional body forces are important. Even the microgravity facilities cannot provide true weightlessness conditions. All facilities suffer from some degree of residual (oscillatory) acceleration whose effects on the considered dynamics have to be carefully assessed prior to planning and executing experiments in space (Lappa and Carotenuto, 2003; Savino and Lappa, 2003).

To study the effect of vibrations on PAS, numerical simulations have been carried out using the Maxey–Riley equation in its *complete* form (Lappa, 2013c) in order to account for the deviations from *the slow manifold* that may be important in strongly time-dependent flows (such as those undergoing the effects of high-frequency g-jitters). Also the effect of the Basset force has been assessed for some configurations.

The results are summarized in Fig. 13 and Fig. 14 for the case of monochromatic vibrations $g(t) = b\omega^2 \sin(\omega t)$ perpendicular and parallel to the axis of the

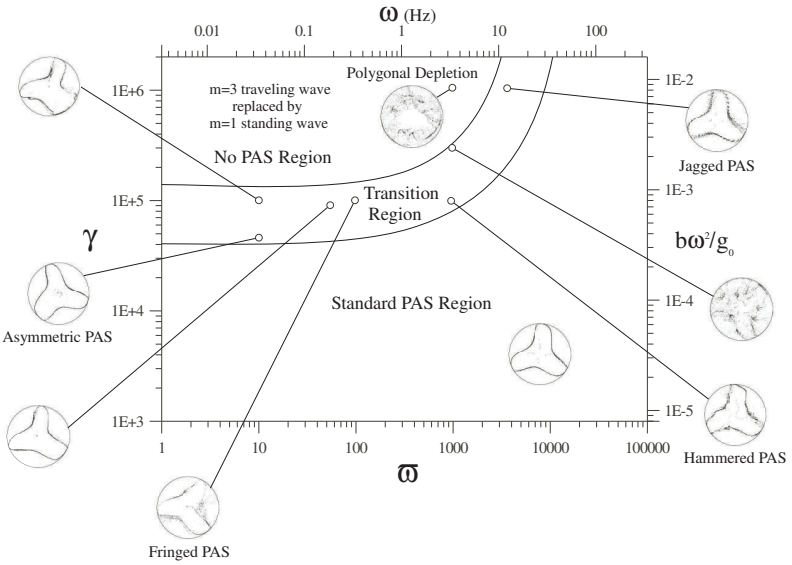

Figure 13: Map for the occurrence of PAS as a function of acceleration amplitude γ and frequency ϖ in the case of g-jitters perpendicular to the axis of the liquid bridge ($\mathrm{Pr} = 8$, $\Gamma = 0.68$, $\mathrm{Ma} = 20600$, density and size of the particles are assumed to be fixed: $\rho = 1.85$, $\mathrm{St} = 10^{-4}$ (Lappa, 2013c). PAS Legend: asymmetric (PAS that has lost its original symmetry characterized by identical lobes), fringed (PAS displaying particles fluctuating in a certain neighborhood of the ideal line which would be formed without vibrations), hammered (PAS displaying a polygon-like shape), jagged (PAS formed by the ordered association of clots of particles), D-PAS (PAS featured by the coexistence of two distinct loops), P-PAS (PAS pulsating in time).

liquid bridge, respectively. The existence of different particle accumulation patterns is shown in the plane spanned by the non-dimensional vibration frequency $\varpi = \omega d^2 \kappa^{-1}$, where b is the vibration amplitude and ω its dimensional angular frequency, and the acceleration amplitude $\gamma = b\omega^2 d^3 \kappa^{-2}$. Depending on the specific conditions, these additional forces can prevent PAS formation at all (see the *no-PAS* region in both figures). In all cases considered there exist, between the limiting regular and irregular particle patterns in space (and/or time), numerous intermediate situations which depend on the applied frequency and amplitude of the vibration.

A more in-depth analysis has revealed both small and large scale structures of the

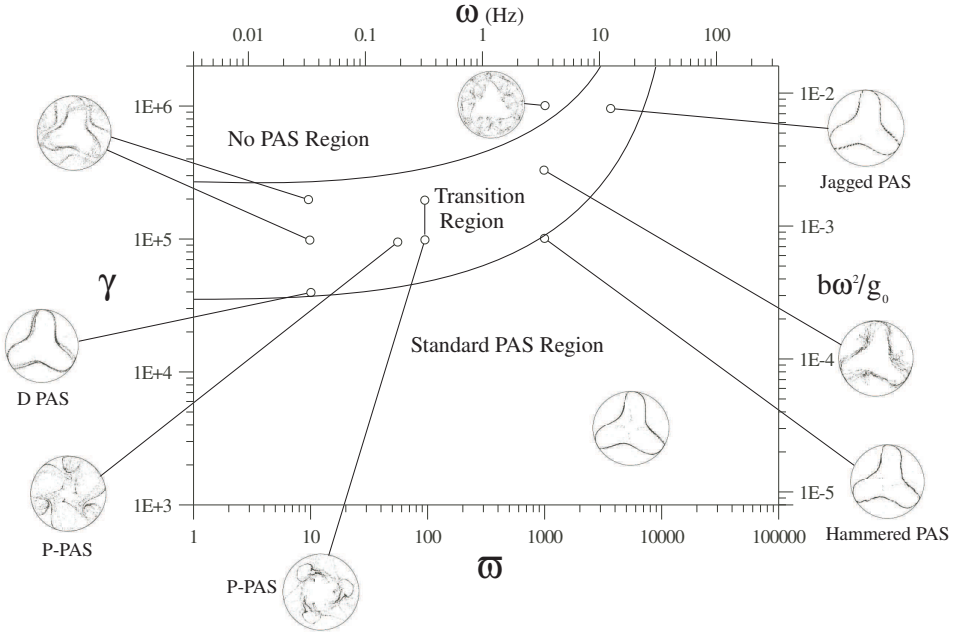

Figure 14: Map for the occurrence of PAS as a function of acceleration amplitude and frequency in the case of g-jitters parallel to the axis of the liquid bridge (refer to fig. 13 for the parameters). PAS legend as in Fig. 13.

particle patterns. This has led to the introduction of a whole zoo of perturbed PAS modes which have been assigned exotic names like asymmetric, fringed, hammered and jagged PAS, pulsating, double PAS, etc. (Lappa, 2013c). Such a categorization has been introduced on the basis of the spatial and temporal scales of the prevailing disturbance and its typical manifestation in the reference frame rotating at the same angular velocity of the traveling thermo-fluid-dynamic wave.

In general, it has been found that both large and small scale defects, appearing, respectively, as asymmetries in the shape of PAS and turbulent displacements of localized sets of particles, can affect PAS dynamics at intermediate values of the vibration frequency. A more precise assessment of the impact of the non-dimensional g-jitter frequency ϖ and amplitude γ, however, has revealed that for a fixed value of γ a first regime exists where the amplitude of the large-scale disturbance is almost constant and independent of ϖ. As the vibration frequency gets larger, the large-scale disturbance is taken over by disturbances on a smaller scale, consisting of a time-periodic departure of particles from the purely one-dimensional PAS that would be obtained in the absence of vibrations. A further increase of ϖ, however,

tends to suppress the small-scale dynamics leading to a full recovery of the classical unperturbed PAS. By contrast, an increase of γ at a constant value of ϖ causes an amplification of both small and large scale defects until all particles become uncorrelated above a certain $\gamma(\varpi)$ (the aforementioned no PAS region).

4 Conclusions

The organization of particles into different coherent dynamic accumulation structures is a surprisingly fast process in thermocapillary flows. To date, a multitude of different particle accumulation patterns has been found, both experimentally and numerically. All these particle patterns rotate with the same angular velocity as the underlying traveling hydrothermal wave.

We have reported the ranges of Marangoni numbers for which different forms of line-like PAS (SL-1, SL-2, low-Ma) exist in 2 cSt-silicone-oil liquid bridges. Furthermore, examples have been given for the phase relation between PAS and the temperature field of the hydrothermal wave, which differs for different liquids employed. These experimental data represent important properties of PAS which ultimately have to be reproduced by numerical modeling.

The current status of different explanations of PAS proposed by the various research groups involved in the JEREMI project has been presented. The respective explanations are based on

- a pure nonlinear systems approach in which PAS is simply an attracting periodic orbit,
- the particular structure of the vorticity field of the hydrothermal wave, or
- the phase-locking between particles and the hydrothermal wave.

In this regard it should be mentioned that, as no generally-accepted theory has been established as yet, not all authors subscribe to all points of view presented in this paper. Since the mechanism of PAS is still a controversial subject, refined experimental investigations and improved numerical modeling are required to develop a consistent theory of PAS formation.

On the experimental side, the measurement accuracy must be further improved. An important step in this direction is the JEREMI experiment which, owing to the much larger length scales and removal of the hydrostatic pressure as well as buoyancy, will allow high accuracy measurements for clearly-defined boundary conditions, in particular, for precisely defined thermal conditions at the interface (see part B of this paper, Shevtsova and et al. (2014)). A correspondingly *clean* space

experiment is a necessary condition to enable a quantitative comparison with numerical simulations. However, not only the accuracy of the experiments must be improved. In addition, new and creative measurement techniques must be developed and employed to prove the existence or absence of PAS and to measure the structure and the dynamics of the various features of PAS predicted by the participating numerical research groups.

On the numerical side, high accuracy computations are required to minimize all sources of numerical error. In addition, the models for the fluid motion must be refined, in particular, with regard to numerical resolution, variable material properties, interfacial deformations, and thermal boundary conditions, to name only the most important factors influencing the flow and PAS. Furthermore, more accurate models for the transport of suspended particles must be employed which take into account the differing behavior of particles when they approach boundaries versus when they are far from boundaries. In this regard it should be noted that the Maxey–Riley equation (Maxey and Riley, 1983) is valid only for particles far from boundaries.

By presenting the current different explanation models for PAS formation it is hoped to stimulate further investigations by other independent researchers in order to ultimately arrive at the correct understanding of the origin of this fascinating phenomenon.

Acknowledgement: We gratefully acknowledge support from JAXA and from ESA in the framework of the project IAO-2000-091 *Dynamics of suspended particles in periodic vortex flows*. H. C. K., F. H. M. and R. V. M. gratefully acknowledge support from ESA (contract number 4000103003) and from ZID of TU Wien. I. U. acknowledges financial support by the Japan Society for the Promotion of Science (JSPS) through a *Grant-in-Aid for Scientific Research (B)* (project number 24360078). He also thanks Y. (Abe) Konisho, H. Enomoto, A. Kawazoe, N. Hattori, Y. Niigaki and T. Sano for setting-up and improving the liquid-bridge experiment. M. L. gratefully acknowledges support from ASI (contract I/048/11/0).

References

Abe, Y.; Ueno, I.; Kawamura, H. (2009): Dynamic particle accumulation structure due to thermocapillary effect in noncylindrical half-zone liquid bridge. *Ann. N. Y. Acad. Sci.*, vol. 1161, pp. 240–245.

Arnold, V. I. (1983): *Geometrical Methods in the Theory of Ordinary Differential Equations*, volume 250 of *Fundamental Principles of Mathematical Sciences*. Springer-Verlag, New York.

Babiano, A.; Cartwright, J. H. E.; Piro, O.; Provenzale, A. (2000): Dynamics of a small neutrally buoyant sphere in a fluid and targeting in Hamiltonian systems. *Phys. Rev. Lett.*, vol. 84, pp. 5764–5767.

Busse, F. H. (1978): Non-linear properties of thermal convection. *Rep. Prog. Phys.*, vol. 41, pp. 1929–1967.

Chun, C.-H.; Wuest, W. (1979): Experiments on the transition from steady to oscillatory Marangoni convection in a floating zone under reduced gravity effect. *Acta Astronautica*, vol. 6, pp. 1073–1082.

Haller, G.; Sapsis, T. (2008): Where do inertial particles go in fluid flows? *Physica D*, vol. 237, pp. 573–583.

Hofmann, E.; Kuhlmann, H. C. (2011): Particle accumulation on periodic orbits by repeated free surface collisions. *Phys. Fluids*, vol. 23, pp. 0721106–1–0721106–14.

Kamotani, Y.; Wang, L.; Hatta, S.; Wang, A.; Yoda, S. (2003): Free surface heat loss effect on oscillatory thermocapillary flow in liquid bridges of high Prandtl number fluids. *Intl J. Heat Mass Transfer*, vol. 46, pp. 3211–3220.

Kawamura, H.; Nishino, K.; Matsumoto, S.; Ueno, I. (2010): Space experiment of Marangoni convection on International Space Station. In *Proceedings of the 14th International Heat Transfer Conference*. ASME.

Kawamura, H.; Nishino, K.; Matsumoto, S.; Ueno, I. (2012): Report on microgravity experiments of marangoni convection aboard international space station. *Journal of Heat Transfer*, vol. 134, no. 3, pp. 031005.

Kawamura, H.; Ueno, I.; Ishikawa, T. (2002): Study of thermocapillary flow in a liquid bridge towards an on-orbit experiment at International Space Station. *Adv. Space Res.*, vol. 29, pp. 611–618.

Kawamura, H.; Ueno, I.; Tanaka, S.; Nagano, D. (2001): Oscillatory, chaotic and turbulent thermocapillary convections in a half-zone liquid bridge. In *2nd International Symposium on Turbulence and Shear-Flow Phenomena*, volume 3, pp. 375–380, Stockholm.

Kuhlmann, H. C. (1999): *Thermocapillary Convection in Models of Crystal Growth*, volume 152 of *Springer Tracts in Modern Physics*. Springer, Berlin, Heidelberg.

Kuhlmann, H. C.; Muldoon, F. H. (2012a): Comment on "Ordering of small particles in one-dimensional coherent structures by time-periodic flows". *Phys. Rev. Lett.*, vol. 108, no. 24, pp. 249401.

Kuhlmann, H. C.; Muldoon, F. H. (2012b): Particle-accumulation structures in periodic free-surface flows: Inertia versus surface collisions. *Phys. Rev.* E, vol. 85, pp. 046310–1–046310–5.

Kuhlmann, H. C.; Nienhüser, C. (2002): Dynamic free-surface deformations in thermocapillary liquid bridges. *Fluid Dyn. Res.*, vol. 31, pp. 103–127.

Kuhlmann, H. C.; Nienhüser, C. (2003): The influence of static and dynamic free-surface deformations on the three-dimensional thermocapillary flow in liquid bridges. In Narayanan, R.; Schwabe, D.(Eds): *Interfacial fluid dynamics and transport processes*, volume 628 of *Lecture Notes in Physics*, pp. 213–239. Springer, Berlin, Heidelberg.

Lappa, M. (2003): Three-dimensional numerical simulation of Marangoni flow instabilities in floating zones laterally heated by an equatorial ring. *Phys. Fluids*, vol. 15, pp. 776–789.

Lappa, M. (2005): Analysis of flow instabilities in convex and concave floating zones heated by an equatorial ring under microgravity conditions. *Comput. Fluids*, vol. 34, pp. 743–770.

Lappa, M. (2010): *Thermal Convection: Patterns, Evolution and Stability*. John Wiley, Chichester, England.

Lappa, M. (2012): *Rotating Thermal Flows in Natural and Industrial Processes*. John Wiley, Chichester, England.

Lappa, M. (2013): Assessment of the role of axial vorticity in the formation of particle accumulation structures in supercritical Marangoni and hybrid thermocapillary-rotation-driven flows. *Phys. Fluids*, vol. 25, pp. 012101–1–012101–11.

Lappa, M. (2013): On the existence and multiplicity of one-dimensional solid particle attractors in time-dependent Rayleigh–Bénard convection. *Chaos*, vol. 23, pp. 013105–1–013105–9.

Lappa, M. (2013): On the variety of particle accumulation structures under the effect of g-jitters. *J. Fluid Mech.*, vol. 726, pp. 160–195.

Lappa, M.; Carotenuto, R. (2003): Effect of convective disturbances induced by g-jitter on the periodic precipitation of lysozyme. *Microgravity Sci. Technol.*, vol. 14, pp. 41–56.

Lappa, M.; Savino, R. (2002): 3D analysis of crystal/melt interface shape and Marangoni flow instability in solidifying liquid bridges. *J. Comput. Phys.*, vol. 180, pp. 751–774.

Lappa, M.; Savino, R.; Monti, R. (2000): Influence of buoyancy forces on Marangoni flow instabilities in liquid bridges. *Int. J. Num. Meth. Heat Fluid Flow*, vol. 10, pp. 721–749.

Leypoldt, J.; Kuhlmann, H. C.; Rath, H. J. (2000): Three-dimensional numerical simulation of thermocapillary flows in cylindrical liquid bridges. *J. Fluid Mech.*, vol. 414, pp. 285–314.

Maxey, M. R.; Riley, J. J. (1983): Equation of motion for a small rigid sphere in a nonuniform flow. *Phys. Fluids*, vol. 26, pp. 883–889.

Melnikov, D.; Pushkin, D.; Shevtsova, V. (2011): Accumulation of particles in time-dependent thermocapillary flow in a liquid bridge. modeling of experiments. *Eur. Phys. J. Special Topics*, vol. 192, no. 1, pp. 29–39.

Mukin, R.; Kuhlmann, H. C. (2013): Topology of hydrothermal waves in liquid bridges and dissipative structures of transported particles. *Phys. Rev.* E, vol. 88, pp. 053016–1–053016–20.

Muldoon, F. H.; Kuhlmann, H. C. (2013a): Coherent particulate structures by boundary interaction of small particles in confined periodic flows. *Physica D*, vol. 253, pp. 40–65.

Muldoon, F. H.; Kuhlmann, H. C. (2013b): Numerical error in modeling of particle accumulation structures in periodic free-surface flows. *Comput. Fluids*, vol. 88, pp. 43–50.

Neitzel, G. P.; Chang, K. T.; Jankowski, D. F.; Mittelmann, H. D. (1993): Linear-stability theory of thermocapillary convection in a model of the float-zone crystal-growth process. *Phys. Fluids A*, vol. 5, pp. 108–114.

Niigaki, Y.; Ueno, I. (2012): Formation of particle accumulation structure (PAS) in half-zone liquid bridge under an effect of thermo-fluid flow of ambient gas. *Trans. Jap. Soc. Aeronaut. Space Sci.*, vol. 10, pp. Ph33–Ph37.

Nishimura, M.; Ueno, I.; Nishino, K.; Kawamura, H. (2005): 3D PTV measurement of oscillatory thermocapillary convection in half-zone liquid bridge. *Exp. Fluids*, vol. 38, pp. 285–290.

Ottino, J. M. (1989): *The Kinematics of Mixing: Stretching, Chaos, and Transport*. Cambridge Texts in Applied Mathematics. Cambridge University Press, Cambridge.

Pikovsky, A.; Rosenblum, M.; Kurths, J. (2003): *Synchronization: A Universal Concept in Nonlinear Sciences*. Cambridge Nonlinear Science Series. Cambridge University Press, Cambridge.

Pushkin, D.; Melnikov, D. E.; Shevtsova, V. M. (2012): A reply to the comment by H. C. Kuhlmann and F. H. Muldoon. *Phys. Rev. Lett.*, vol. 108, pp. 249402–1 – 2.

Pushkin, D. O.; Melnikov, D. E.; Shevtsova, V. M. (2011): Ordering of small particles in One-Dimensional coherent structures by Time-Periodic flows. *Phys. Rev. Lett.*, vol. 106, no. 23, pp. 234501–1–234501–4.

Rhines, P. B. (1975): Waves and turbulence on a beta-plane. *J. Fluid Mech.*, vol. 69, pp. 417–443.

Sato, F.; Ueno, I.; Kawamura, H.; Nishino, K.; Matsumoto, S.; Ohnishi, M.; Sakurai, M. (2013): Hydrothermal wave instability in a high-aspect-ratio liquid bridge of $Pr > 200$. *Microgravity Sci. Technol.*, vol. 25, pp. 43–58.

Savino, R.; Lappa, M. (2003): Assessment of the thermovibrational theory: application to g-jitter on the space-station. *Journal of Spacecraft and Rockets*, vol. 40, pp. 201–210.

Schuster, H. G. (1984): *Deterministic chaos: An introduction*. VCH Publishers, Weinheim.

Schwabe, D.; Hintz, P.; Frank, S. (1996): New features of thermocapillary convection in floating zones revealed by tracer particle accumulation structures (PAS). *Microgravity Sci. Technol.*, vol. 9, pp. 163–168.

Schwabe, D.; Mizev, A. I.; Udhayasankar, M.; Tanaka, S. (2007): Formation of dynamic particle accumulation structures in oscillatory thermocapillary flow in liquid bridges. *Phys. Fluids*, vol. 19, pp. 072102–1–072102–18.

Schwabe, D.; Preisser, F.; Scharmann, A. (1982): Verification of the oscillatory state of thermocapillary convection in a floating zone under low gravity. *Acta Astronautica*, vol. 9, pp. 265–273.

Schwabe, D.; Scharmann, A. (1979): Some evidence for the existence and magnitude of a critical Marangoni number for the onset of oscillatory flow in crystal growth melts. *J. Crystal Growth*, vol. 46, pp. 125–131.

Schwabe, D.; Scharmann, A.; Preisser, F.; Oeder, F. (1978): Experiments on surface tension driven flow in floating zone melting. *J. Crystal Growth*, vol. 43, pp. 305–312.

Schwabe, D.; Tanaka, S.; Mizev, A.; Kawamura, H. (2006): Particle accumulation structures in time-dependent thermocapillary flow in a liquid bridge under microgravity conditions. *Microgravity Sci. Technol.*, vol. 18, pp. 117–127.

Shevtsova, V.; Mialdun, A.; Kawamura, H.; Ueno, I.; Nishino, K.; Lappa, M. (2011): Onset of hydrothermal instability in liquid bridge. Experimental benchmark. *Fluid Dyn. Mater. Process.*, vol. 7, pp. 1–28.

Shevtsova, V. M.; et al. (2014): The JEREMI-project on thermocapillary convection in liquid bridges. part B: Control of thermocapillary convection by a coaxial gas flow. *Fluid Dyn. Mater. Process.*, pg. submitted.

Shevtsova, V. M.; Melnikov, D. E.; Legros, J. C. (2001): Three-dimensional simulations of hydrodynamic instability in liquid bridges: Influence of temperature-dependent viscosity. *Phys. Fluids*, vol. 13, pp. 2851–2865.

Smith, M. K.; Davis, S. H. (1983): Instabilities of dynamic thermocapillary liquid layers. Part 1. Convective instabilities. *J. Fluid Mech.*, vol. 132, pp. 119–144.

Tanaka, S.; Kawamura, H.; Ueno, I.; Schwabe, D. (2006): Flow structure and dynamic particle accumulation in thermocapillary convection in a liquid bridge. *Phys. Fluids*, vol. 18, pp. 067103–1–067103–11.

Ueno, I.; Kawazoe, A.; Enomoto, H. (2009): Effect of ambient-gas forced flow on oscillatory thermocapillary convection of half-zone liquid bridge. *Fluid Dyn. Mat. Proc.*, vol. 229, no. 1, pp. 1–10.

Ueno, I.; Ono, Y.; Nagano, D.; Tanaka, S.; Kawamura, H. (2000): Modal oscillatory structure and dynamic particle accumulation in liquid-bridge Marangoni convection. In *4th JSME–KSME Thermal Engineering Conference*, pp. 3–265–3–270, Kobe, Japan. Japanese Society of Mechanical Engineers.

Ueno, I.; Tanaka, S.; Kawamura, H. (2003): Oscillatory and chaotic thermocapillary convection in a half-zone liquid bridge. *Phys. Fluids*, vol. 15, pp. 408–416.

Wanschura, M.; Shevtsova, V. S.; Kuhlmann, H. C.; Rath, H. J. (1995): Convective instability mechanisms in thermocapillary liquid bridges. *Phys. Fluids*, vol. 7, pp. 912–925.

Yano, T.; Nishino, K.; Kawamura, H.; Ueno, I.; Matsumoto, S.; Ohnishi, M.; Sakurai, M. (2011): Space experiment on the instability of Marangoni convection in large liquid bridge - MEIS-4: effect of Prandtl number. *Journal of Physics: Conference Series*, vol. 327, pp. 012029.